Published OnlineFirst May 2, 2018; DOI: 10.1158/1535-7163.MCT-17-0645

Large Molecule Therapeutics

Molecular Cancer Therapeutics

A Raf-Competitive K-Ras Binder Can Fail to Functionally Antagonize Signaling

Monique J. Kauke[1,2], Alison W. Tisdale[2,3], Ryan L. Kelly[2,3], Christian J. Braun[2,4], Michael T. Hemann[2,4], and K. Dane Wittrup[1,2,3]

Abstract

Mutated in approximately 30% of human cancers, Ras GTPases are the most common drivers of oncogenesis and render tumors unresponsive to many standard therapies. Despite decades of research, no drugs directly targeting Ras are currently available. We have previously characterized a small protein antagonist of K-Ras, R11.1.6, and demonstrated its direct competition with Raf for Ras binding. Here we evaluate the effects of R11.1.6 on Ras signaling and cellular proliferation in a panel of human cancer cell lines. Through lentiviral transduction, we generated cell lines that constitutively or through induction with doxycycline express R11.1.6 or a control protein YW1 and show specific binding by R11.1.6 to endogenous Ras through microscopy and co-immunoprecipitation experiments. Genetically encoded intracellular expression of this high-affinity Ras antagonist, however, fails to measurably disrupt signaling through either the MAPK or PI3K pathway. Consistently, cellular proliferation was unaffected as well. To understand this lack of signaling inhibition, we quantified the number of molecules of R11.1.6 expressed by the inducible cell lines and developed a simple mathematical model describing the competitive binding of Ras by R11.1.6 and Raf. This model supports a potential mechanism for the lack of biological effects that we observed, suggesting stoichiometric and thermodynamic barriers that should be overcome in pharmacologic efforts to directly compete with downstream effector proteins localized to membranes at very high effective concentrations. *Mol Cancer Ther; 17(8); 1773–80.* *©2018 AACR.*

Introduction

K-Ras, H-Ras, and N-Ras are small GTPases that regulate key cellular processes including proliferation, migration, and survival. Nucleotide loading with either GTP or GDP defines the conformation of the switch I and switch II regions of Ras proteins and thereby their state of activation (1–3). Active, GTP-bound Ras binds effector proteins including Raf (4) and PI3K (5) to initiate downstream signaling. Upon hydrolysis of GTP, Ras adopts an inactive, GDP-bound conformation that leads to termination of signaling.

The Ras proteins comprise the most frequently mutated family of oncoproteins in all human cancers, including three of the most lethal forms, cancers of the lung, colon, and pancreas. Oncogenic Ras mutations, such as those at positions G12, G13, and Q61, impair intrinsic Ras activity (6), preventing GTP hydrolysis and resulting in constitutively active Ras capable of binding and signaling through downstream effector proteins. This leads to cell transformation, proliferation, and eventual migration and invasion (1–3).

Given its high level of incidence across a large subset of cancer types and its well-established role in tumor initiation, development, and progression, a large effort has been put forth in Ras inhibitor development. But despite decades of research and a renewed enthusiasm in recent years, no clinically approved drugs directly targeting Ras are currently available, primarily due to its disordered active site and smooth surface lacking well-defined drug-binding pockets (2, 3). Although small-molecule inhibitors of Ras are low in their binding affinity and efficacy (3, 7–9), antagonists developed on protein scaffolds have greater ability to specifically and tightly interact with the smooth protein. Indeed, several protein-based Ras inhibitors have been developed (10–14) and have shown varying degrees of preclinical efficacy.

We previously described a protein inhibitor R11.1.6, which was engineered on a scaffold based on the thermostable protein Sso7d (15) and was shown to exhibit preferential binding to K-Ras G12D over wild-type (16). Extensive characterization of the binding interaction between R11.1.6 and K-Ras G12D indicated direct competition of R11.1.6 with downstream effector Raf, which led to inhibition of mutant K-Ras–induced signaling through the MAPK pathway in a model system. Here we evaluate the effects of R11.1.6-mediated endogenous K-Ras antagonism on a panel of human cancer cell lines and show an unexpected absence of signaling inhibition or reduction in cellular proliferation. To help understand this apparently contradictory outcome, we propose a simple mathematical model describing R11.1.6 binding of K-Ras in the presence of Raf, demonstrating that pharmacologic efforts toward competitive Ras antagonism may be met with intrinsic challenges.

[1]Department of Chemical Engineering, Massachusetts Institute of Technology, Cambridge, Massachusetts. [2]Koch Institute for Integrative Cancer Research, Massachusetts Institute of Technology, Cambridge, Massachusetts. [3]Department of Biological Engineering, Massachusetts Institute of Technology, Cambridge, Massachusetts. [4]Department of Biology, Massachusetts Institute of Technology, Cambridge, Massachusetts.

Note: Supplementary data for this article are available at Molecular Cancer Therapeutics Online (http://mct.aacrjournals.org/).

Corresponding Author: K. Dane Wittrup, Massachusetts Institute of Technology, 500 Main Street 76-261, Cambridge, MA 02139. Phone: 617-253-4578; Fax: 617-253-1954; E-mail: wittrup@mit.edu

doi: 10.1158/1535-7163.MCT-17-0645

Published OnlineFirst May 2, 2018; DOI: 10.1158/1535-7163.MCT-17-0645

Materials and Methods

Reagents

Western blot antibodies were anti-vinculin (13901S), anti-pMEK1/2 (Ser217/221; 9121S), anti-MEK1/2 (9122S), anti-pERK p44/42 (Thr202/Tyr204; 9101S), anti-ERK (9102S), anti-pAKT (Ser473; 9271S), anti-AKT (9272S), anti-Ras (3339S), and anti-GFP (2555S) from Cell Signaling Technology. Blots were detected with an horseradish peroxidase–conjugated secondary antibody (406401) from BioLegend. Wortmannin (W1628-1MG; ref. 17) was purchased from Sigma and ZSTK474 (18) was a kind gift from Dr. Forest White at Massachusetts Institute of Technology (Boston, MA).

Cell culture

HEK 293T (obtained from ATCC in 2016), A431 (obtained from ATCC in 2013), PA-TU-8902 (kind gift from Dr. Mandar Muzumdar, Jacks Lab, Massachusetts Institute of Technology, Cambridge, MA, in 2017), and PA-TU-8988T (kind gift from Dr. Mandar Muzumdar, Jacks Lab, Massachusetts Institute of Technology, in 2017) cells were cultured in DMEM. HT-29 (obtained from ATCC in 2013) and Calu-1 (obtained from ATCC in 2012) cells were cultured in McCoy 5A. HPAF-II (obtained from ATCC in 2015) and LS180 (obtained from ATCC in 2013) cells were cultured in Eagle minimum essential medium. NCI-H23 (obtained from ATCC in 2012), SW48 WT, SW48 G12D, SW48 G12C, and SW48 G12V (all SW48 cell lines were kind gifts from the White Lab, Massachusetts Institute of Technology, in 2016; ref. 19) were cultured in RPMI1640. All media were supplemented with 10% FBS (Life Technologies), 100 U/mL penicillin, and 100 μg/mL streptomycin (Life Technologies) and were purchased from ATCC and Life Technologies. Cell lines transduced to stably express R11.1.6, YW1, EGFP, or EGFP fusions of R11.1.6/YW1 were cultured in the media as indicated above. Cell lines transduced to express EGFP fusions of R11.1.6/YW1 under an inducible promoter were cultured in the media as indicated above, but without penicillin/streptomycin and with Tet System Approved FBS (Clontech) and 1 to 4 μg/mL puromycin (Life Technologies). All cell lines were maintained at 37°C and 5% CO_2 and were authenticated by the manufacturer and tested for mycoplasma contamination to meet standard levels. Cell lines were passaged a minimum of five times and up to fifteen times before use.

Subcloning

For constitutive expression, R11.1.6 and YW1 were cloned into lentiviral vector pLJM1-EGFP (Addgene plasmid #19319) using In-Fusion Cloning (Clontech) according to the manufacturer's instructions. Cmyc-R11.1.6 and cmyc-YW1 were cloned into a modified version of the lentiviral vector pLJM1, in which protein expression is under the CMV promoter and EGFP under the PGK promoter, using In-Fusion Cloning (Clontech) according to the manufacturer's instructions. For inducible expression, the sequences for EGFP-R11.1.6 and EGFP-YW1 were PCR amplified, digested with *Age*I and *Nhe*I, and cloned into *Age*I- and *Nhe*I-digested lentiviral pCW57.1 (Addgene plasmid #41393) vector. Cloning and DNA preparations were done using One Shot Stbl3 cells (Thermo Fisher Scientific).

Lentivirus generation, transduction, and cell line selections

To generate VSV-G pseudotyped lentiviral particles using the pLJM1 and modified pLJM1 expression plasmids, second-generation packaging plasmids were used. HEK 293T cells were transiently transfected in 10-cm plates with pLJM1 or modified pLJM1 plasmids (into which had been cloned cmyc- or EGFP-R11.1.6 or -YW1) and packaging plasmids using calcium phosphate. Approximately 24 hours after transfection, media containing virus particles were harvested and filtered through a 0.45-μm filter. To generate VSV-G pseudotyped lentiviral particles using the pCW57.1 doxycycline-inducible expression plasmid, third-generation packaging plasmids were used. HEK 293T cells were transiently transfected in 10-cm plates with pCW57.1 plasmid (into which had been cloned EGFP-R11.1.6 or -YW1) and packaging plasmids using Fugene transfection reagent (Roche). After approximately 72 hours, media containing virus particles were harvested and centrifuged to remove cell debris.

To transduce cancer cell lines with pLJM1 lentiviral particles, cells to be infected were plated in 12-well plates and adhered overnight. Filtered virus harvested from the HEK 293T transient transfection was added at 1 mL/well and incubated for approximately 24 hours, after which virus-containing media were replaced with complete media as described above. To transduce cancer cell lines with pCW57.1-inducible lentiviral particles, cells to be infected were plated in 6-well plates and adhered overnight. Centrifuged virus harvested from the HEK 293T transient transfection was added at 0.5 mL/well to 1 mL/well complete media supplemented with polybrene (Sigma) at 5 μg/mL final concentration. Cells were transduced overnight at 37°C.

To select successfully transduced cells with the pLJM1 viral particles, cells were sorted either once or twice based on EGFP expression using a FACSAria IIU (BD Biosciences). Successfully transduced cells with the inducible pCW57.1 viral particles were selected using puromycin (Life Technologies) at 4 or 5 μg/mL final concentration. Selected cells were induced with doxycycline (Sigma) for 48 hours and read on a BD ACCURI C6 flow cytometer for EGFP expression. Flow cytometry data were analyzed using FlowJo software.

Quantitative PCR

Expression of R11.1.6 and YW1 in the pLJM1-based stable cell lines was verified using qRT-PCR. RNA extraction was done using the NucleoSpiný RNA Midi Kit (Clontech) according to the manufacturer's instructions. RT-PCR and amplification were then performed using the QuantiTect SYBR Green RT-PCR Kit (Qiagen) according to the manufacturer's instructions, on a Roche Lightcycler 480 (Roche). The forward primer for R11.1.6/YW1 used was 5′-TTATTTCTGAAGAGGACTTGGGA-3′, and the reverse 5′-CCAACGGATTACCCACTTG-3′. β-Actin was used as the housekeeping gene, with the forward primer of 5′-GTCTGCCTTGGTAGTGGATAATG-3′ and the reverse primer of 5′-TCGAGGACGCCCTATCATGG-3′.

Fluorescence microscopy

Lentivirus-generated stable cell lines were plated on #1 glass cover slips (Chemglass) and adhered overnight. Approximately 24 hours after plating, cells were fixed with 4% paraformaldehyde for 10 minutes at room temperature and coverslips mounted with DAPI-containing mounting medium (Vectashield, Vector Laboratories) and dried overnight. Lentivirus-generated inducible stable cell lines were plated on #1 glass coverslips (Chemglass) and adhered overnight. Cells were induced with doxycycline (Sigma) at 2 μg/mL final concentration for 48 hours and then fixed with 4% paraformaldehyde for 10 minutes at room temperature and

Published OnlineFirst May 2, 2018; DOI: 10.1158/1535-7163.MCT-17-0645

cover slips mounted with DAPI-containing mounting medium (Vectashield, Vector Laboratories) and dried overnight. Images were acquired at room temperature using a GE (Applied Precision) DeltaVision Spectris inverted Olympus X71 microscope with a 60× objective lens, captured with a Photometrics CoolSNAP HQ camera. SoftWoRx software was used for image acquisition and deconvolution. EGFP signal used the ex. 475/em. 528 filter set.

Cell signaling assay

Lentivirus-generated stable cell lines were plated and adhered overnight, and then serum-starved overnight. Human EGF (PeproTech) was added at a final concentration of 1 nmol/L for 5 minutes, after which cells were washed on ice and lysed in protease inhibitor (cOmplete EDTA-free protease inhibitor cocktail; Roche) containing RIPA lysis buffer (Abcam). Lentivirus-generated inducible stable cell lines were plated and adhered overnight. Cells were induced with doxycycline (Sigma) at 125, 250, 500, 1,000, or 2,000 ng/mL final concentration for 48 hours at 37°C. Cells were washed on ice and lysed in protease inhibitor (cOmplete EDTA-free protease inhibitor cocktail; Roche) containing RIPA lysis buffer (Abcam). Whole-cell lysates were analyzed by Western blot analysis for activation of MEK, ERK, and/or AKT with phosphospecific antibodies.

Proliferation assay

Stable cell line proliferation was measured using a WST-1–based colorimetric assay according to the manufacturer's instructions (Roche). Cells were seeded in flat-bottom 96-well plates and incubated for 24, 48, or 72 hours at 37°C and 5% CO_2, after which proliferation was determined. In some assays, PI3K inhibitors wortmannin (Sigma) or ZSTK474 (kind gift from the White Lab; Massachusetts Institute of Technology) were added to cells for 24 hours, after which proliferation was determined.

Clonogenic assay

Colony formation of the stable cell lines was evaluated by seeding cells at 10,000 cells/well in 6-well plates and incubating them at 37°C and 5% CO_2 until sufficiently large colonies (approximately 30–50 cells/colony) had formed, about 2 to 3 weeks. Once colonies had formed, they were stained with a mixture of 6.0% glutaraldehyde (Sigma) and 0.5% crystal violet (Sigma) for 30 minutes at room temperature.

Co-immunoprecipitation assay

Inducible stable cell lines were seeded in a 10-cm plate and adhered overnight, then induced with doxycycline (Sigma) at 3,000 ng/mL final concentration for 48 hours at 37°C. Cells were washed on ice and lysed in protease inhibitor (cOmplete EDTA-free protease inhibitor cocktail; Roche) containing lysis buffer (Life Technologies). Whole-cell lysates were analyzed by Western blot analysis for total Ras and EGFP-R11.1.6/YW1. EGFP-R11.1.6/YW1 were pulled down with anti-GFP beads (ChromoTek) and analyzed for co-immunoprecipitation of Ras by Western blotting.

R11.1.6 quantification

To determine the number of EGFP-R11.1.6 molecules expressed in the inducible cell lines, we quantified both total mass of protein via Western blot analysis and fluorescence of EGFP via flow cytometry. Inducible stable cell lines were plated and adhered overnight, then induced with doxycycline (2,000 ng/mL) for 48 hours at 37°C. Cells were detached and counted, then washed and lysed in protease inhibitor (cOmplete EDTA-free protease inhibitor cocktail; Roche) containing RIPA lysis buffer (Abcam). Volumes of whole-cell lysates equaling 5×10^4 cells were analyzed by Western blot analysis with anti-GFP antibody (Cell Signaling Technology), and the number of EGFP-R11.1.6 molecules per cell quantified using ImageJ software and a standard curve of recombinant GFP (Abcam). For quantification based on fluorescence, we utilized GFP flow cytometer calibration beads (Clontech) according to the manufacturer's instructions. We plated and induced cell lines as above and read them on a BD ACCURI C6 flow cytometer for EGFP expression. Flow cytometry data were analyzed using FlowJo software.

Mathematical model

To model the degree of R11.1.6-mediated inhibition of complexes between K-Ras and Raf, we utilized a simple competitive binding inhibition model analogous to Michaelis–Menten–based derivations for competitive enzyme inhibitors (Fig. 3A; Supplementary Fig. S4). Rather than defining degree of inhibition of K-Ras by R11.1.6 as the fraction of K-Ras occupied by R11.1.6 (Supplementary Fig. S6A), we describe it as the number of K-Ras–Raf complexes that are prevented from forming by the presence of R11.1.6 (Supplementary Fig. S6B–S6D). The number of R11.1.6 and Raf molecules in the cell was varied for a given number of K-Ras molecules in our simulations to obtain heatmaps as shown in Fig. 3 and Supplementary Fig. S7.

Results

Intracellular expression of R11.1.6 has no apparent effect on cancer cell signaling and proliferation

Our recent engineering and characterization of R11.1.6, a novel protein antagonist that specifically binds mutant K-Ras G12D with single-digit nanomolar affinity, showed a Ras binding epitope that is directly competitive with downstream effector Raf (16). Taking advantage of the ease of transfection of HEK 293T cells, we utilized this model system to show strong inhibition of signaling through the MAPK pathway in the presence of R11.1.6. To extend these findings to more relevant settings, we generated stable human cancer cell lines to constitutively express R11.1.6 or the control protein YW1 (in which two of the R11.1.6 paratope residues have been swapped to abrogate K-Ras binding; ref. 16), either with an EGFP reporter or as EGFP fusions (Supplementary Fig. S1A). We confirmed the expression of R11.1.6/YW1 in the EGFP reporter cell lines via quantitative RT-PCR (Supplementary Fig. S1B).

Human cancer cell lines HT-29 (colorectal, K-Ras WT), LS180 (colorectal, K-Ras G12D), and HPAF-II (pancreatic, K-Ras G12D) stably expressing EGFP fusions of R11.1.6 show clear peripheral membrane staining, consistent with binding to Ras, which localizes to the inner plasma membrane (Fig. 1A). Diffuse cytoplasmic fluorescence further indicates that sufficient excess of the EGFP-R11.1.6 fusion is present to avoid significant depletion upon binding to membrane-localized Ras. This membrane localization is not observed for control cell lines expressing EGFP-YW1 or EGFP only. We next investigated the effects of R11.1.6 expression on endogenous Ras-driven signaling (Fig. 1B). Curiously, we observed no inhibition in either the MAPK or PI3K pathway, as evidenced by no changes in phosphorylation of MEK, ERK, or AKT (Ser473) in the presence of R11.1.6. This lack of signaling

Published OnlineFirst May 2, 2018; DOI: 10.1158/1535-7163.MCT-17-0645

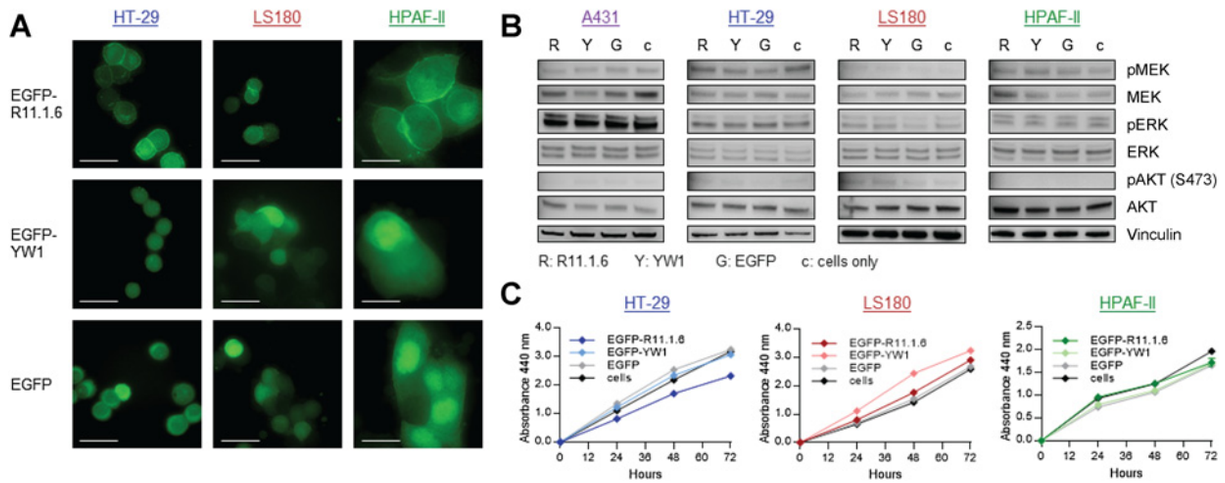

Figure 1.

Constitutive intracellular expression of R11.1.6 has no apparent effect on cancer cell signaling and proliferation. **A,** Fluorescence microscopy of human cancer cell lines HT-29 (K-Ras WT), LS180 (K-Ras G12D), and HPAF-II (K-Ras G12D) transduced to constitutively express EGFP-tagged R11.1.6, EGFP-tagged control YW1, or EGFP only. Scale bars, 30 μm. **B,** Western blots probing phosphorylation of endogenous MEK (pMEK), ERK (pERK), and AKT at Ser473 (pAKT) in human cancer cell lines A431 (K-Ras WT), HT-29 (K-Ras WT), LS180 (K-Ras G12D), and HPAF-II (K-Ras G12D), constitutively expressing R11.1.6, YW1, or EGFP. **C,** Proliferation, as measured by absorbance at 440 nm, of cell lines as in **A** over 72 hours.

inhibition expectedly translated into unchanged levels of cellular proliferation (Fig. 1C), ability to form colonies (Supplementary Fig. S2A), and growth in soft agar. We thought that combination of R11.1.6-mediated Ras antagonism and PI3K inhibition via small-molecule inhibitors wortmannin and ZSTK474 may result in greater slowing of growth for the R11.1.6-expressing cell lines compared with controls, but found that across a range of concentrations of added inhibitor, there was no difference in proliferation between the cell lines attributable to R11.1.6 expression (Supplementary Fig. S2B).

We observed that cell lines transduced to stably express R11.1.6 maintained EGFP signal over the course of 30 days (Supplementary Fig. S2C), suggesting that presence of R11.1.6 does not affect proliferation even after considerable time has passed. Because cancer cells are known to develop resistance to chemotherapy and targeted therapy (20) and have been shown to upregulate alternative pathways in response to targeted inhibitors (21), we hypothesized that the cell lines had circumvented R11.1.6 antagonism through amplification of other pathways. To mitigate the potential for resistance inherent in constitutive expression, we expanded our panel of human cancer cell lines (Table 1) and generated stable cell lines that express EGFP fusions of R11.1.6 or YW1 under an inducible promoter, so that only upon addition of doxycycline is there cytoplasmic expression.

Table 1. Human cancer cell lines for inducible EGFP-R11.1.6/YW1 expression

Cell line	Tissue	K-Ras
A431	Skin	WT
HT-29	Colon	WT
SW48 WT	Colon	WT
LS180	Colon	G12D
HPAF-II	Pancreas	G12D
SW48 G12D	Colon	G12D
Calu-1	Lung	G12C
NCI-H23	Lung	G12C
SW48 G12C	Colon	G12C
SW48 G12V	Colon	G12V
PA-TU-8902	Pancreas	G12V
PA-TU-8988T	Pancreas	G12V

Selected cell lines showed no leaky expression in the absence of doxycycline and induction of EGFP-fused proteins at the highest doxycycline concentration (Supplementary Fig. S3). Consistent with our constitutively expressing stable cell lines (Fig. 1A), we observed membrane localization in the panel of inducible cell lines expressing EGFP-R11.1.6, but not the EGFP-YW1 control (Fig. 2A). Specific binding to Ras was confirmed by coimmunoprecipitation, showing that the cell lines induced to express EGFP-R11.1.6 pull down Ras whereas those expressing EGFP-YW1 do not (Fig. 2B). Having confirmed binding of Ras by R11.1.6, we next investigated its effects on downstream signaling, probing for phosphorylation of ERK 48 hours following induction of expression (Fig. 2C). Again, we failed to observe any inhibition of signaling in response to R11.1.6-mediated Ras antagonism, even at the highest concentrations of doxycycline.

Mathematical model of competitive binding of Ras by R11.1.6 and Raf

In an effort to try to understand the lack of signaling inhibition, we developed a simple mathematical model to describe the system in which R11.1.6 competes with downstream effector proteins for binding of K-Ras (Fig. 3A; Supplementary Fig. S4). For our analysis, we define Raf as the model downstream effector because it has the highest affinity for K-Ras, in the double-digit nanomolar range (ref. 22; compared with low micromolar affinity for PI3K; refs. 23, 24; and RalGDS; ref. 25), and therefore is the greatest competitor for R11.1.6 binding. We then utilized this model to evaluate the feasibility of R11.1.6 inhibiting a significant portion of the K-Ras–Raf complexes that drive downstream signaling.

To determine the degree of inhibition possible as predicted by our model, we needed to quantify the number of copies of EGFP-R11.1.6 expressed by the cells upon induction with doxycycline. Quantification of fluorescence yielded an average across all cell

Published OnlineFirst May 2, 2018; DOI: 10.1158/1535-7163.MCT-17-0645

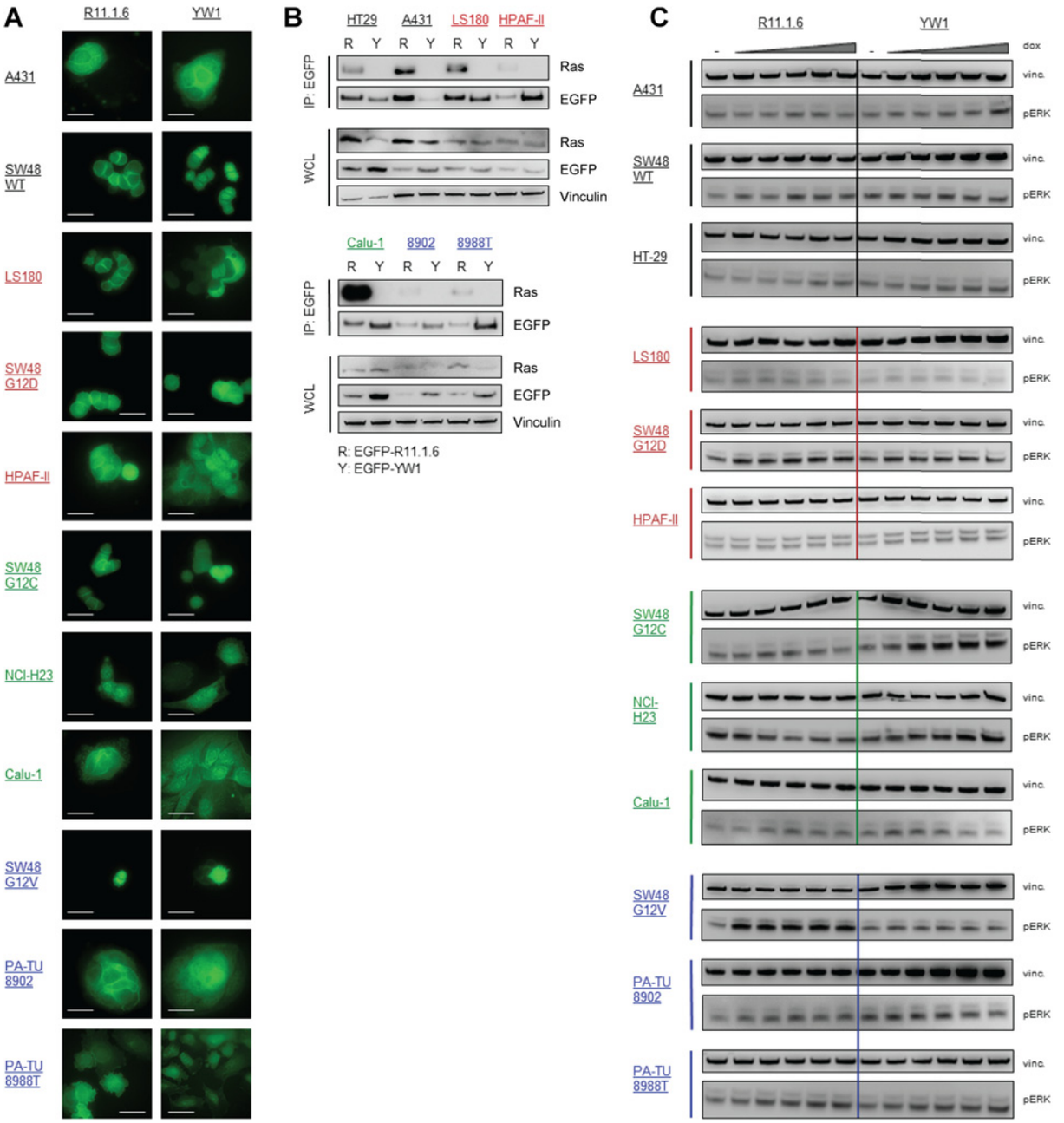

Figure 2.

Inducible intracellular expression of R11.1.6 has no effect on ERK phosphorylation in cancer cell lines. **A,** Fluorescence microscopy of the human cancer cell lines listed in Table 1, induced with doxycycline for 48 hours to express EGFP-tagged R11.1.6 or EGFP-tagged control YW1. Scale bars, 30 μm. **B,** Coimmunoprecipitation of Ras with EGFP-tagged R11.1.6/YW1 in inducible cell lines after 48 hours of induction with doxycycline. IP, immunoprecipitation; WCL, whole-cell lysate. **C,** Western blots probing phosphorylation of endogenous ERK in inducible cell lines after 48 hours of induction with doxycycline. Increasing final doxycycline concentrations shown are 125, 250, 500, 1,000, and 2,000 ng/mL.

lines of 1.3×10^6 molecules of EGFP-R11.1.6 per cell (Fig. 3B; Supplementary Fig. S5A), which we confirmed by also quantifying based on quantitative Western blots (Supplementary Fig. S5B and S5C).

Rather than defining the degree of inhibition as the fraction of K-Ras molecules occupied by R11.1.6 (Supplementary Fig. S6A), we normalized the number of K-Ras–Raf complexes that form in the presence of a given number of R11.1.6 molecules to the number that form if no inhibitor is present and defined this as the fraction of complexes that remain intact (Supplementary Fig. S6B and S6C). From this we then calculated the fraction of complexes that are inhibited by R11.1.6

Published OnlineFirst May 2, 2018; DOI: 10.1158/1535-7163.MCT-17-0645

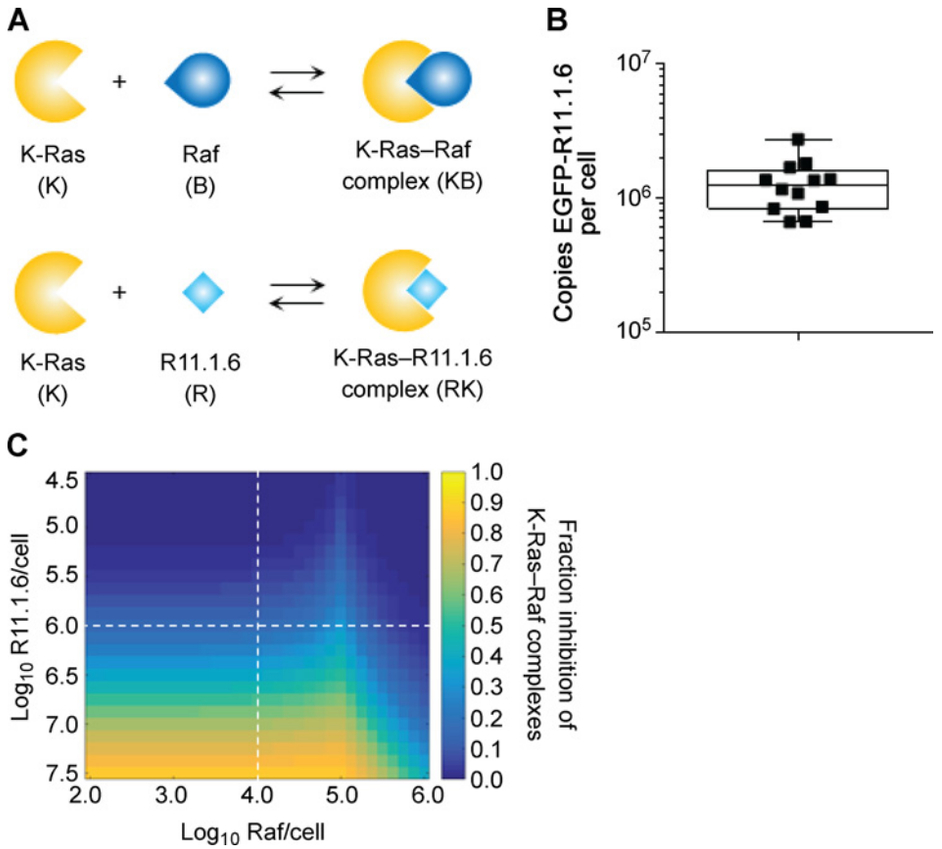

Figure 3.
Model of Raf-competitive K-Ras antagonism by R11.1.6 offers insight into lack of effects on cancer cells. **A,** Schematic of mathematical model using mass action kinetics to describe the competitive binding of K-Ras by R11.1.6 and downstream effector Raf. **B,** Quantification of the total number of copies of EGFP-tagged R11.1.6 per cell in each of the inducible cancer cell lines. Each point represents the average of $n = 3$ replicates. Individual cell line quantifications are given in Supplementary Fig. S5A. **C,** Model-derived heatmap depicting the fraction of inhibition of K-Ras–Raf complex formation by R11.1.6 as a function of the total number of Raf and R11.1.6 molecules per cell. Simulation held the number of K-Ras molecules constant at 10^5 molecules per cell. Dotted lines indicate the average number of EGFP-R11.1.6 molecules per cell as measured in **B** and the number of Raf molecules per cell as presented in the literature (26).

(Supplementary Fig. S6D). Simulation over a range of Raf and R11.1.6 numbers per cell, with the number of K-Ras molecules held constant at 10^5 per cell (26), yields a heatmap of R11.1.6-mediated inhibition of K-Ras–Raf complex formation (Fig. 3C). At approximately 10^6 copies of EGFP-R11.1.6 per cell and 10^4 copies of Raf (26), our model predicts only 16% inhibition of the K-Ras–Raf complexes that would otherwise form. This then could explain our negative results for signal inhibition with both the constitutively expressing and inducible cell lines, where we observed membrane localization of R11.1.6 (Figs. 1A and 2A) and were able to coimmunoprecipitate Ras (Fig. 2B) but failed to see signaling inhibition at the pERK level (Figs. 1B and 2C). We postulate that the binding of R11.1.6 to Ras was sufficient to detect in our assays but perhaps insufficient to alter signaling.

Of course, no mathematical model can prove a hypothesis to be correct—it is simply a way to test for consistency of particular mechanisms with available data. Our purpose in constructing the presented model is to determine whether the previously demonstrated (27–31) membrane localization of Ras effectors such as Raf are sufficient to result in incomplete competitive antagonism by R11.1.6. Comparing antagonism in the presence (Fig. 3C) or absence (Supplementary Fig. S7) of this Raf localization effect, it is clear that our data are consistent with such a hypothesis for a wide range of potential Raf and R11.1.6 concentrations.

Modeling of the MAPK cascade has shown ERK to be ultrasensitive in its stimulus–response curve (32). Furthermore, pERK and pAKT have both been shown to be highly sensitive to upstream EGF stimulation, with significant signal amplification measured in response to minimal input (33). Because Ras-driven signaling is amplified as the cascade proceeds, we propose that inhibition of the upstream input be near-complete to observe detectable changes downstream. The partial inhibition predicted for R11.1.6 by our simulations therefore would not suffice, which is consistent with our cell line–based data.

Discussion

We previously described the engineering and characterization of R11.1.6, a high-affinity protein antagonist of K-Ras–Raf interaction (16). In this work, we utilized R11.1.6 as a genetically encoded tool to evaluate the effects of Raf-competitive Ras antagonism in a panel of human cancer cell lines and found that despite measurable binding to endogenous Ras, R11.1.6 fails to inhibit signaling through both the MAPK and PI3K pathways. We developed a simple mathematical model describing the competition for Ras binding between R11.1.6 and downstream effector Raf and predicted that at the level of cytoplasmic R11.1.6 expression attained in our stable cell lines, only 16% inhibition of the K-Ras–Raf complexes that drive signaling may be achieved.

Although our model can help explain the absence of R11.1.6-mediated signaling inhibition that we observed, it should be noted that the simulation is strongly dependent on the adjustment of K-Ras–Raf binding made to account for the high local concentration of Raf (Supplementary Fig. S4B). Upon activation of Ras, either due to extracellular stimuli or mutation, Raf is

Published OnlineFirst May 2, 2018; DOI: 10.1158/1535-7163.MCT-17-0645

recruited to the plasma membrane (27–31), its local concentration significantly increases driving interaction with Ras and initiation of downstream signaling. It has been shown that 1,000-fold increases in local concentration of factors such as Sos are achieved due to membrane localization, and that these increases drive Ras signaling (34). So in our model, we approximated the impact of Raf localization by adjusting the on-rate ($k_{on,Raf}$) for the second binding event in bivalent binding at a surface (35) while assuming the off-rate ($k_{off,Raf}$) is unchanged. This effective on-rate ultimately determines the degree of inhibition that can be achieved, which in the absence of Raf localization would be approximately 97% (Supplementary Fig. S7). Our model, therefore, suggests that the special feature of a very high local concentration of native ligand may make the pharmacologic objective of competitive antagonism challenging.

Our observations propose that Raf-competitive Ras antagonism may be difficult, and although several small-molecule and protein-based inhibitors have been shown to exert effects on Ras-driven signaling and proliferation, these do not necessarily conflict with our conclusions here. Small molecules that directly block interaction of Ras with Raf bind with weak affinity and exert their effects at concentrations in the hundreds of micromolar range (7–9). Such high concentrations may translate into drug molecules on the order of 10^7 per cell, at which point our simulation predicts near complete inhibition (Fig. 3C). Our own characterization of R11.1.6 in the model HEK 293T system showed significant signaling inhibition, but only when plasmid encoding R11.1.6 was transfected at greater amounts than plasmid encoding K-Ras G12D (16). A recent self-internalizing antibody that blocks Ras interaction with downstream effector proteins showed efficacy in both cell-based assays and murine xenograft models (14). Again, micromolar concentrations were required to observe effects, the bivalent IgG format may increase avidity significantly, and it is possible the antibody constant region contributed function via intracellular Fc receptors, analogous to that observed for intracellular antibody-bound pathogens (36). Finally, a single antibody VH domain engineered to bind mutant H-Ras was shown to compete with effector proteins, but only exhibited efficacy when a membrane-localizing peptide was appended (12).

Pharmacologic inhibition of Ras-driven tumors continues to be challenging, and although significant progress has been made over the years, the Ras problem is far from solved. Our findings may help shed light on a particular difficulty of interrupting this signaling axis and the potential hurdles that must be overcome in competitive Ras antagonism. Perhaps alternative approaches, such as allosteric antagonists (13), covalent allele-specific G12C inhibitors (37, 38), or immunotherapy (39), are likely to have greater chances of success given this possible fundamental issue.

Disclosure of Potential Conflicts of Interest

No potential conflicts of interest were disclosed.

Authors' Contributions

Conception and design: M.J. Kauke, K.D. Wittrup
Development of methodology: M.J. Kauke, R.L. Kelly, C.J. Braun
Acquisition of data (provided animals, acquired and managed patients, provided facilities, etc.): M.J. Kauke, R.L. Kelly
Analysis and interpretation of data (e.g., statistical analysis, biostatistics, computational analysis): M.J. Kauke, A.W. Tisdale, K.D. Wittrup
Writing, review, and/or revision of the manuscript: M.J. Kauke, K.D. Wittrup
Administrative, technical, or material support (i.e., reporting or organizing data, constructing databases): C.J. Braun
Study supervision: M.J. Kauke, M.T. Hemann, K.D. Wittrup

Acknowledgments

Funding for M.J. Kauke and A.W. Tisdale came from NIH grant 5-R01-CA096504-15, the MIT Associate Director Fund, and the MIT Frontier Fund. We would also like to acknowledge the generous gift from an anonymous donor to make this study possible. This work was further supported by the Koch Institute Support (core) grant P30-CA14051 from the NCI. R.L. Kelly and A.W. Tisdale were supported by a graduate fellowship from the National Institute of General Medical Sciences Interdepartmental Biotechnology Training Program at the NIH (T32 GM008334-25). C.J. Braun was supported by a Mildred-Scheel fellowship from the German Cancer Foundation and the MIT Ludwig Center for Cancer Research. We would like to thank D. Sabatini for pLJM1-EGFP (Addgene plasmid #19319), D. Root for pCW57.1 (Addgene plasmid #41393), and D. Trono for pMDLg/pRRE (Addgene plasmid #12251), pRSV-Rev (Addgene plasmid #12253), and pMD2.G (Addgene plasmid #12259). We thank Mandar Muzumdar and Tyler Jacks for the PA-TU-8902 and PA-TU-8988T cell lines, and Forest White for the isogenic SW48 WT, G12D, G12C, and G12V cell lines and the ZSTK474 PI3K inhibitor. We also thank the Koch Institute Swanson Biotechnology Center for technical support, specifically the Flow Cytometry and Microscopy Core Facilities.

The costs of publication of this article were defrayed in part by the payment of page charges. This article must therefore be hereby marked *advertisement* in accordance with 18 U.S.C. Section 1734 solely to indicate this fact.

Received July 10, 2017; revised November 15, 2017; accepted April 23, 2018; published first May 2, 2018.

References

1. Cox AD, Der CJ. Ras history: the saga continues. Small GTPases 2010;1:2–27.
2. Stephen AG, Esposito D, Bagni RK, McCormick F. Dragging Ras back in the ring. Cancer Cell 2014;25:272–81.
3. Cox AD, Fesik SW, Kimmelman AC, Luo J, Der CJ. Drugging the undruggable RAS: mission possible? Nat Rev Drug Discov 2014;13:828–51.
4. Moodie SA, Willumsen BM, Weber MJ, Wolfman A. Complexes of Ras.GTP with Raf-1 and mitogen-activated protein kinase kinase. Science 1993;260:1658–61.
5. Rodriguez-Viciana P, Warne PH, Dhand R, Vanhaesebroeck B, Gout I, Fry MJ, et al. Phosphatidylinositol-3-OH kinase as a direct target of Ras. Nature 1994;370:527–32.
6. Trahey M, McCormick F. A cytoplasmic protein stimulates normal N-Ras p21 GTPase, but does not affect oncogenic mutants. Science 1987;238:542–5.
7. Karaguni IM, Glüsenkamp KH, Langerak A, Geisen C, Ullrich V, Winde G, et al. New indene-derivatives with anti-proliferative properties. Bioorg Med Chem Lett 2002;12:709–13.
8. Kato-Stankiewicz J, Hakimi I, Zhi G, Zhang J, Serebriiskii I, Guo L, et al. Inhibitors of Ras/Raf-1 interaction identified by two-hybrid screening revert Ras-dependent transformation phenotypes in human cancer cells. Proc Natl Acad Sci U S A 2002;99:14398–403.
9. Shima F, Yoshikawa Y, Ye M, Araki M, Matsumoto S, Liao J, et al. In silico discovery of small-molecule Ras inhibitors that display antitumor activity by blocking the Ras-effector interaction. Proc Natl Acad Sci U S A 2013;110:8182–7.
10. Upadhyaya P, Qian Z, Selner NG, Clippinger SR, Wu Z, Briesewitz R, et al. Inhibition of Ras signaling by blocking Ras-effector interactions with cyclic peptides. Angew Chem Int Ed Engl 2015;54:7602–6.

Published OnlineFirst May 2, 2018; DOI: 10.1158/1535-7163.MCT-17-0645

11. Leshchiner ES, Parkhitko A, Bird GH, Luccarelli J, Bellairs JA, Escudero S, et al. Direct inhibition of oncogenic KRAS by hydrocarbon-stapled SOS1 helices. Proc Natl Acad Sci U S A 2015;112:1761–6.
12. Tanaka T, Williams RL, Rabbitts TH. Tumor prevention by a single antibody domain targeting the interaction of signal transduction proteins with RAS. EMBO J 2007;26:3250–9.
13. Spencer-Smith R, Koide A, Zhou Y, Eguchi RR, Sha F, Gajwani P, et al. Inhibition of RAS function through targeting an allosteric regulatory site. Nat Chem Biol 2017;13:62–8.
14. Shin SM, Choi DK, Jung K, Bae J, Kim JS, Park SW, et al. Antibody targeting intracellular oncogenic Ras mutants exerts anti-tumour effects after systemic administration. Nat Commun 2017;8:15090.
15. Traxlmayr MW, Kiefer JD, Srinivas RR, Lobner E, Tisdale AW, Mehta NK, et al. Strong enrichment of aromatic residues in binding sites from a charge-neutralized hyperthermostable Sso7d scaffold library. J Biol Chem 2016;291:22496–508.
16. Kauke MJ, Traxlmayr MW, Parker JA, Kiefer JD, Knihtila R, McGee J, et al. An engineered protein antagonist of K-Ras/B-Raf interaction. Sci Rep 2017;7:5831.
17. Baggiolini M, Dewald B, Schnyder J, Ruch W, Cooper PH, Payne TG. Inhibition of the phagocytosis-induced respiratory burst by the fungal metabolite wortmannin and some analogues. Exp Cell Res 1987;169: 408–18.
18. Yaguchi S, Fukui Y, Koshimizu I, Yoshimi H, Matsuno T, Gouda H, et al. Antitumor activity of ZSTK474, a new phosphatidylinositol 3-kinase inhibitor. J Natl Cancer Inst 2006;98:545–56.
19. Hammond DE, Mageean CJ, Rusilowicz EV, Wickenden JA, Clague MJ, Prior IA. Differential reprogramming of isogenic colorectal cancer cells by distinct activating KRAS mutations. J Proteome Res 2015;14:1535–46.
20. Zahreddine H, Borden KL. Mechanisms and insights into drug resistance in cancer. Front Pharmacol 2013;4:28.
21. Isoyama S, Dan S, Nishimura Y, Nakamura N, Kajiwara G, Seki M, et al. Establishment of phosphatidylinositol 3-kinase inhibitor-resistant cancer cell lines and therapeutic strategies for overcoming the resistance. Cancer Sci 2012;103:1955–60.
22. Fischer A, Hekman M, Kuhlmann J, Rubio I, Wiese S, Rapp UR. B- and C-RAF display essential differences in their binding to Ras: the isotype-specific N terminus of B-RAF facilitates Ras binding. J Biol Chem 2007;282:26503–16.
23. Pacold ME, Suire S, Perisic O, Lara-Gonzalez S, Davis CT, Walker EH, et al. Crystal structure and functional analysis of Ras binding to its effector phosphoinositide 3-kinase gamma. Cell 2000;103:931–43.
24. Fritsch R, de Krijger I, Fritsch K, George R, Reason B, Kumar MS, et al. RAS and RHO families of GTPases directly regulate distinct phosphoinositide 3-kinase isoforms. Cell 2013;153:1050–63.
25. Linnemann T, Kiel C, Herter P, Herrmann C. The activation of RalGDS can be achieved independently of its Ras binding domain. Implications of an activation mechanism in Ras effector specificity and signal distribution. J Biol Chem 2002;277:7831–7.
26. Shi T, Niepel M, McDermott JE, Gao Y, Nicora CD, Chrisler WB, et al. Conservation of protein abundance patterns reveals the regulatory architecture of the EGFR-MAPK pathway. Sci Signal 2016;9:rs6.
27. Rizzo MA, Shome K, Watkins SC, Romero G. The recruitment of Raf-1 to membranes is mediated by direct interaction with phosphatidic acid and is independent of association with Ras. J Biol Chem 2000;275:23911–8.
28. Marais R, Light Y, Paterson HF, Marshall CJ. Ras recruits Raf-1 to the plasma membrane for activation by tyrosine phosphorylation. EMBO J 1995; 14:3136–45.
29. Light Y, Paterson H, Marais R. 14-3-3 antagonizes Ras-mediated Raf-1 recruitment to the plasma membrane to maintain signaling fidelity. Mol Cell Biol 2002;22:4984–96.
30. Ory S, Zhou M, Conrads TP, Veenstra TD, Morrison DK. Protein phosphatase 2A positively regulates Ras signaling by dephosphorylating KSR1 and Raf-1 on critical 14-3-3 binding sites. Curr Biol 2003;13: 1356–64.
31. Improta-Brears T, Ghosh S, Bell RM. Mutational analysis of Raf-1 cysteine rich domain: requirement for a cluster of basic amino acids for interaction with phosphatidylserine. Mol Cell Biochem 1999;198:171–8.
32. Huang CY, Ferrell JE Jr. Ultrasensitivity in the mitogen-activated protein kinase cascade. Proc Natl Acad Sci U S A 1996;93:10078–83.
33. Chen WW, Schoeberl B, Jasper PJ, Niepel M, Nielsen UB, Lauffenburger DA, et al. Input-output behavior of ErbB signaling pathways as revealed by a mass action model trained against dynamic data. Mol Syst Biol 2009;5:239.
34. Groves JT, Kuriyan J. Molecular mechanisms in signal transduction at the membrane. Nat Struct Mol Biol 2010;17:659–65.
35. Wittrup KD, Tidor B. Molecular and cellular bioengineering: rate processes in biological systems. In: Biomolecular kinetics and cellular dynamics. Hamden, CT: Taylor & Francis Inc.; 2014. p. 30–3.
36. McEwan WA, Tam JC, Watkinson RE, Bidgood SR, Mallery DL, James LC. Intracellular antibody-bound pathogens stimulate immune signaling via the Fc receptor TRIM21. Nat Immunol 2013;14:327–36.
37. Ostrem JM, Peters U, Sos ML, Wells JA, Shokat KM. K-Ras(G12C) inhibitors allosterically control GTP affinity and effector interactions. Nature 2013; 503:548–51.
38. Lito P, Solomon M, Li L-S, Hansen R, Rosen N. Allele-specific inhibitors inactivate mutant KRAS G12C by a trapping mechanism. Science 2016; 351:604–8.
39. Tran E, Robbins PF, Lu YC, Prickett TD, Gartner JJ, Jia L, et al. T-cell transfer therapy targeting mutant KRAS in cancer. N Engl J Med 2016;375:2255–62.

Published OnlineFirst May 2, 2018; DOI: 10.1158/1535-7163.MCT-17-0645

Molecular Cancer Therapeutics

A Raf-Competitive K-Ras Binder Can Fail to Functionally Antagonize Signaling

Monique J. Kauke, Alison W. Tisdale, Ryan L. Kelly, et al.

Mol Cancer Ther 2018;17:1773-1780. Published OnlineFirst May 2, 2018.